Design, Modeling and Control of an Omni-Directional Aerial Vehicle

Dario Brescianini and Raffaello D'Andrea

Abstract— In this paper we present the design and control of a novel six degrees-of-freedom aerial vehicle. Based on a static force and torque analysis for generic actuator configurations, we derive an eight-rotor configuration that maximizes the vehicle's agility in any direction. The proposed vehicle design possesses full force and torque authority in all three dimensions. A control strategy that allows for exploiting the vehicle's decoupled translational and rotational dynamics is introduced. A prototype of the proposed vehicle design is built using reversible motor-propeller actuators and capable of flying at any orientation. Preliminary experimental results demonstrate the feasibility of the novel design and the capabilities of the vehicle.

I. INTRODUCTION

Unmanned aerial vehicles are fast becoming a mature technology and have already been successfully used as a tool for various tasks including surveillance, inspection, mapping and search and rescue operations. While these applications make use of the vehicles mobility and unique aerial perspective, several groups have more recently started to investigate the use of flying machines for physical interaction with the environment; to manipulate objects (e.g. [1]–[3]), to assemble structures in locations otherwise inaccessible (e.g. [4]), or to interact with humans and augment reality (e.g. [5], [6]).

Typically, multi-rotor vehicles such as quadrocopters are used to perform these tasks because of their agility and mechanical simplicity. However, these traditional multi-rotor vehicles are under-actuated, i.e. unable to independently control their thrust and torque in all three dimensions. In order to increase performance criteria such as flight duration, payload, or robustness, all rotor disks are aligned in a single plane. This constrains the vehicle's thrust vector to a single direction and thereby coupling the translational and rotational dynamics. The inability of traditional multi-rotor vehicles to point their thrust and torque vector independently in any direction limits their set of feasible position and attitude trajectories and also their ability to physically interact with the environment or to perform complex manipulation tasks as this often requires the vehicles to instantaneously resist arbitrary force and torque disturbances.

To overcome these limitations, several novel multi-rotor vehicle designs have been developed over the past years: In [7] and [8], multi-rotor vehicles with tilting propellers are studied. By adding servos to rotate the vehicle arms around their main axes, the alignment of the rotor disks can be changed and the thrust direction can be chosen arbitrarily. In [9], a configuration with three small-angle

The authors are with the Institute for Dynamic Systems and Control, ETH Zurich, Switzerland. {bdario, rdandrea}@ethz.ch
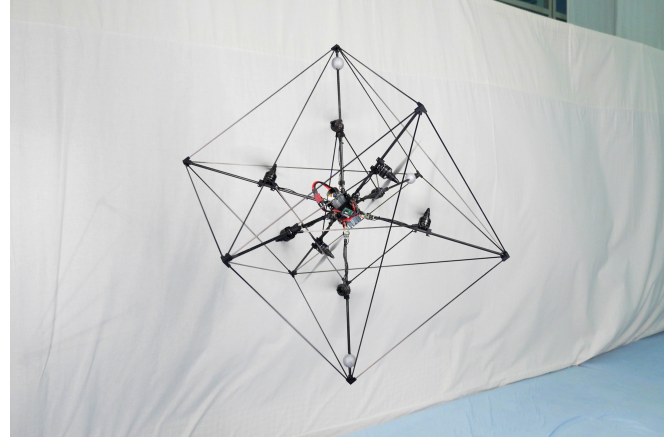
Fig. 1: Image of the omni-directional vehicle described in this paper hovering at an arbitrarily chosen attitude.

adjustable ducted fans mounted horizontally around two large, counter-rotating coaxial propellers is proposed. The large propellers are responsible to generate enough lift to overcome gravity whereas the small ducted fans are used to provide lateral forces. In [10]–[13], hex-rotor vehicle designs are analyzed, where the actuators are arranged in pairs on three different planes such that the plane normals span the three dimensional Euclidean space and any desired thrust and torque combination can be achieved. In [14], a six degrees-of-freedom vehicle is presented where the rotor configuration is the result of an optimization problem. Although all of these vehicles provide independent force and torque control, they all have directions in which substantially more force and torque can be generated than in others in order to efficiently overcome gravity. As a consequence, they are usually not able to fly at arbitrary orientations due to actuator constraints.

In this paper we introduce the design and control of a novel omni-directional multi-rotor aerial vehicle, i.e. a vehicle whose dynamical properties are almost independent of the vehicle orientation and that is able to hover and accelerate in any direction at any attitude (see Fig. 1). The omni-directionality allows the vehicle to fully exploit its decoupled translational and rotational dynamics and renders a novel set of maneuvers feasible.

The remainder of this paper is organized as follows: In Section II, an omni-directional actuator configuration is presented. A dynamic model for the proposed vehicle design is derived in Section III. In Section IV, a control strategy to track arbitrary position and attitude trajectories is introduced. The implementation of the proposed vehicle design and experimental results are presented in Section V, and the paper is concluded in Section VI.

II. Vehicle Design

In this section, we present a six degrees-of-freedom vehicle design based on a static force and torque analysis for generic actuator configurations. The objective is to find an actuator configuration that maximizes the vehicle's agility while rendering its dynamical properties as rotationally invariant as possible. For ease of notation, vectors may be expressed as n-tuples $\boldsymbol{x} = (x_1, x_2, \ldots x_n)$ with dimensions and stacking clear from context. Unless otherwise stated, all three dimensional vectors are expressed in the vehicle's body frame $\mathcal{B}$.

The force and torque analysis is limited to reversible fixed-pitch motor-propeller actuators with fixed rotor disk orientations due to their mechanical simplicity and weight considerations. Reversible motor-propeller actuators have the advantage that both positive and negative thrust can be produced and that the load can therefore be distributed more evenly among all actuators. However, because most brushless motor controllers rely on measuring the motors back electromotive force to estimate the motor position and to control the commutations, a minimum angular rate and hence minimum thrust is required in order for the motors to function properly. The thrust f_{prop} that a propeller can produce is thus constrained to

$$0 < f_{\text{prop,min}} \leq |f_{\text{prop}}| \leq f_{\text{prop,max}}. \tag{1}$$

Although in practice $f_{\text{prop,min}}$ is almost zero, changing the thrust from a positive to a negative value or vice versa takes substantially longer than a thrust change of equal magnitude without reversing (see Fig. 2). Propeller thrusts close to zero should therefore be avoided in practice such that small disturbances do not require the motor to be reversed. However, for the static force and torque analysis in this section, we assume that $f_{\text{prop,min}} = 0$.

If the aerodynamic interference between rotors is neglected, the force $\boldsymbol{f}$ and torque $\boldsymbol{t}$ generated by a generic N-rotor configuration is given by

$$\boldsymbol{f} = \sum_{i=1}^{N} f_{\text{prop,i}} \boldsymbol{x}_i, \tag{2}$$

$$\boldsymbol{t} = \sum_{i=1}^{N} f_{\text{prop,i}} (\boldsymbol{p}_i \times \boldsymbol{x}_i) + \kappa f_{\text{prop,i}} \boldsymbol{x}_i, \tag{3}$$

where $f_{\text{prop,i}}$ is the thrust magnitude generated by rotor i, $\boldsymbol{x}_i$ is the rotor disk normal, $\boldsymbol{p}_i$ is the rotor position relative to the vehicle's center of mass and κ is the propeller specific thrust-to-drag ratio. The first term in (3) represents the torque due to the off-center mounting of the rotors whereas the second term represents the torque induced by the aerodynamic drag of the propeller. Because the latter is typically an order of magnitude smaller, it will be omitted for the remainder of this analysis. The force and torque expressions can then be written as

$$\binom{\boldsymbol{f}}{\boldsymbol{t}} = \binom{\boldsymbol{X}}{\boldsymbol{P} \times \boldsymbol{X}} \boldsymbol{f}_{\text{prop}}, \tag{4}$$
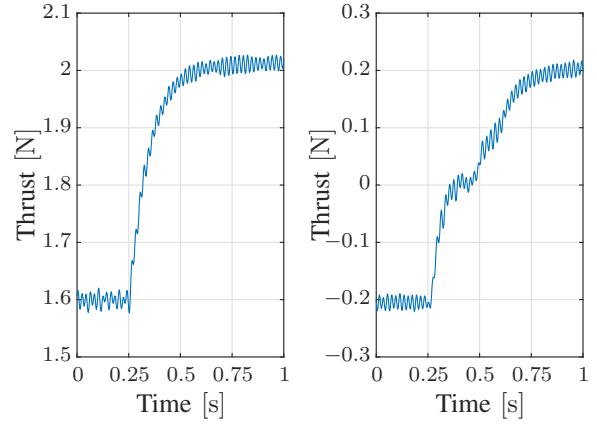

Fig. 2: Thrust response of a reversible motor-propeller actuator to a commanded thrust step of 0.4 N at 0.25 s. The left plot shows a thrust step without reversing the propeller ($t_{90} - t_{10} = 0.20$ s) whereas the right plot shows a thrust step where the spinning direction of the motor reverses ($t_{90} - t_{10} = 0.45$ s).

with $\boldsymbol{X} = (\boldsymbol{x}_1, \boldsymbol{x}_2, \ldots \boldsymbol{x}_N)$, $\boldsymbol{P} = (\boldsymbol{p}_1, \boldsymbol{p}_2, \ldots \boldsymbol{p}_N)$, $\boldsymbol{f}_{\text{prop}} = (f_{\text{prop,1}}, f_{\text{prop,2}}, \ldots f_{\text{prop,N}})$ and with the i-th column of $\boldsymbol{P} \times \boldsymbol{X}$ being defined to be $\boldsymbol{p}_i \times \boldsymbol{x}_i$. Furthermore, let $\boldsymbol{M}$ be the matrix that maps the propeller thrusts $\boldsymbol{f}_{\text{prop}}$ to force and torque $\boldsymbol{y} = (\boldsymbol{f}, \boldsymbol{t})$, i.e.

$$\boldsymbol{y} = \boldsymbol{M} \boldsymbol{f}_{\text{prop}}. \tag{5}$$

In order for the vehicle to be able to independently control its force and torque in any direction, $\boldsymbol{M}$ must have full rank and therefore the number of actuators has to be greater or equal to six.

Because we want the vehicle's dynamical characteristics to be as independent of its orientation as possible, we require the vehicle's inertia tensor to be rotationally invariant. Let $\boldsymbol{J}$ denote the vehicle's inertia tensor with respect to its body frame and let $\boldsymbol{J}'$ be the inertia tensor described in a coordinate frame that is rotated by any rotation matrix $\boldsymbol{R}$ with respect to the body frame. $\boldsymbol{J}'$ is then given by

$$\boldsymbol{J}' = \boldsymbol{R} \boldsymbol{J} \boldsymbol{R}^T. \tag{6}$$

If we require that the inertia tensor is rotationally invariant, i.e. $\boldsymbol{J}' = \boldsymbol{J}$ for all $\boldsymbol{R} \in SO(3)$, then (6) implies that $\boldsymbol{J}\boldsymbol{R} = \boldsymbol{R}\boldsymbol{J}$ and accordingly that the inertia tensor is a multiple of the identity matrix, i.e. all principle moments of inertia are equal. In [15], it is proven that the inertia tensor only reduces to a multiple of the unit tensor for solids that have at least two n-fold rotational axes (with $n \geq 3$). Consequently, if we assume that the vehicle's inertia tensor is mainly determined by the actuator positions and that the actuators can be approximated by point masses, then the set of actuator positions has to satisfy the same criterion. Points which satisfy this are the vertices of regular solids of which the smallest three sets of points are the vertices of a regular tetrahedron ($N = 4$), the vertices of a regular octahedron ($N = 6$) and the vertices two arbitrary aligned regular tetrahedra whose centers coincide ($N = 8$) [16]. Because at least six actuators are required, we limit the

(a) $N = 6$, $r_{\max} = 1.41$ (b) $N = 8$ (two tetrahedra), $r_{\max} = 2.66$ (c) $N = 8$ (cube), $r_{\max} = 2.31$
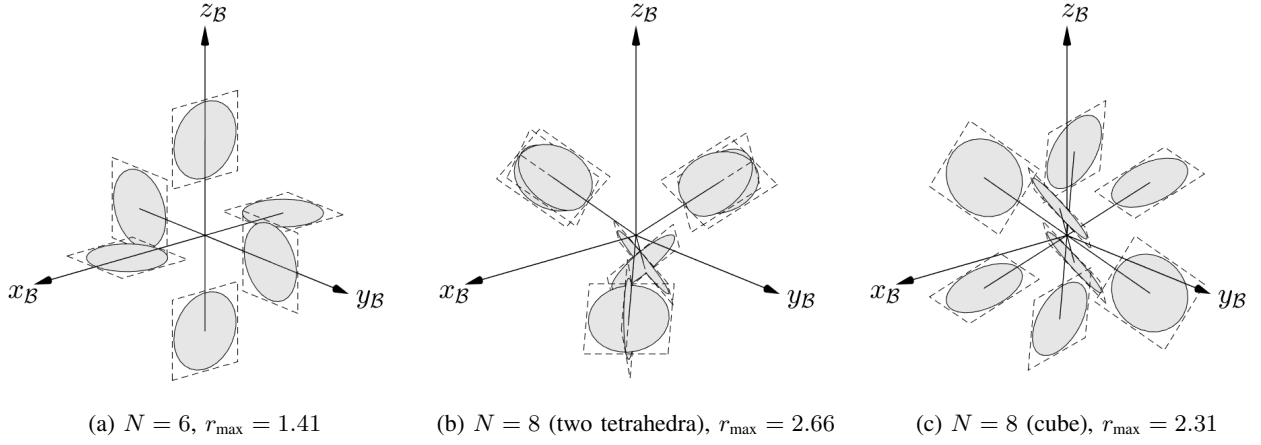
Fig. 3: Actuator configurations obtained by numerically solving the optimization problem (8). Fig. 3a and 3b illustrate solutions with the actuator positions constrained to the vertices of a regular octahedron and of two arbitrary aligned regular tetrahedra with coinciding centers, respectively. However, for the sake of realizability, we decided on an actuator configuration with the actuator positions fixed to the vertices of a cube (see Fig. 3c). For a maximum propeller thrust of $f_{\mathrm{prop,max}} = 1$, the configurations are able produce a force-torque output in any direction with 2-norm of at least $r_{\max} = 1.41$, $r_{\max} = 2.66$ and $r_{\max} = 2.31$, respectively.

actuator positions to the latter two sets. Note that all points in these sets are equidistant from the center. Without loss of generality, we choose the actuators to lie on the unit sphere, $\|\boldsymbol{p}_{\mathrm{i}}\|_2 = 1$, such that the torques are normalized and an actuator thrust of one unit results at most in one unit of torque.

The rotor disk orientations are obtained by maximizing the vehicle's agility, where the 2-norm of the maximum attainable force-torque output in any direction is used as a measure for the vehicle's agility. Let $\mathcal{Y}$ be the set of attainable forces and torques,

$$\mathcal{Y} = \{\boldsymbol{M}\boldsymbol{f}_{\mathrm{prop}} \mid \|\boldsymbol{f}_{\mathrm{prop}}\|_\infty \le f_{\mathrm{prop,max}}\}. \tag{7}$$

The actuator configuration design problem for a given $\boldsymbol{P}$ can then be written as

$$
\begin{aligned}
&\underset{\boldsymbol{X}}{\text{maximize}} \quad \arg\max_r\{r : \{\boldsymbol{y} \mid \|\boldsymbol{y}\|_2 \le r\} \subseteq \mathcal{Y}\} \\
&\text{subject to} \quad \|\boldsymbol{x}_{\mathrm{i}}\|_2 = 1, \ i = 1, \ldots, N.
\end{aligned}
\tag{8}
$$

Solutions obtained through a numerical optimization with the positions fixed to the vertices of a regular octahedron and of two regular tetrahedra are depicted in Fig. 3a and 3b, respectively. It can be seen that the rotor disks are aligned perpendicular to their position vector in order to maximize the torque output for a given propeller thrust. Because the set of admissible propeller thrusts (1) is in practice not connected, the set of attainable forces and torques can only be connected if $\boldsymbol{M}$ has a non-trivial null space. An actuator configuration is thus only able to generate forces and torques in any direction if the number of actuators is larger than six. Although not all configurations with the actuator positions limited to the vertices of two tetrahedra obtain an equally large maximum 2-norm of attainable forces and torques, we decided, for the sake of realizability and due to its many symmetries, on a configuration with the actuators fixed to the vertices of a cube as depicted in Fig. 3c, with the position

and orientation matrices $\boldsymbol{P}$ and $\boldsymbol{X}$ given by

$$
\boldsymbol{P} = \frac{1}{\sqrt{3}}
\begin{pmatrix}
1 & -1 & 1 & -1 & 1 & -1 & 1 & -1 \\
1 & 1 & -1 & -1 & 1 & 1 & -1 & -1 \\
1 & 1 & 1 & 1 & -1 & -1 & -1 & -1
\end{pmatrix}, \tag{9}
$$

$$
\boldsymbol{X} =
\begin{pmatrix}
-a & b & -b & a & a & -b & b & -a \\
b & a & -a & -b & -b & -a & a & b \\
c & -c & -c & c & c & -c & -c & c
\end{pmatrix}, \tag{10}
$$

with $a = 1/2 + 1/\sqrt{12}$, $b = 1/2 - 1/\sqrt{12}$ and $c = 1/\sqrt{3}$. In comparison to the unconstrained solution, this configuration has a 13.4% smaller maximum 2-norm of attainable forces and torques. An analysis of the null space of this configuration showed that the set of attainable forces and torques is connected if

$$f_{\mathrm{prop,min}} \le \frac{f_{\mathrm{prop,max}} - f_{\mathrm{prop,min}}}{2}. \tag{11}$$

III. DYNAMICS

In this section, we derive a model for the dynamics of the proposed omni-directional vehicle with the propeller thrusts $\boldsymbol{f}_{\mathrm{prop}}$ as control inputs. Because of the non-planar configuration and tight arrangement of rotors, complex aerodynamic effects such as interference between rotors or induced velocity are likely to have a substantial effect on the vehicle dynamics for non-steady flight. However, modeling these effects is a very challenging task and is considered to be beyond the scope of this paper. Instead, we use a first-principles model based on the force and torque equations introduced in Section II and treat the secondary aerodynamic effects as disturbances.

We introduce a body-fixed coordinate frame $\mathcal{B}$ with its origin at the vehicle's center of mass as illustrated in Fig. 4. The vehicle's translational degrees-of-freedom are described by the position of the vehicle's center of mass $\boldsymbol{p} = (p_{\mathrm{x}} \ p_{\mathrm{y}} \ p_{\mathrm{z}})$, expressed in an inertial frame $\mathcal{I}$, and its
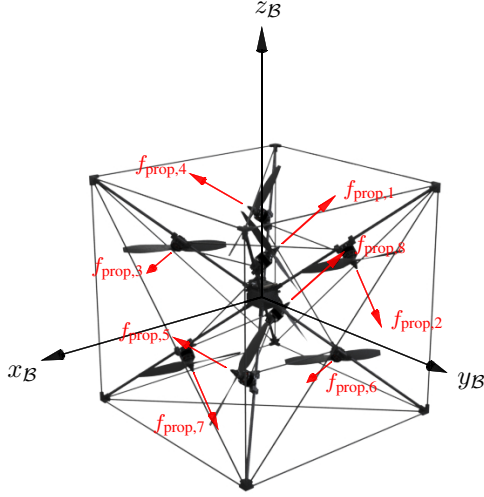
Fig. 4: Illustration of the proposed omni-directional vehicle design with its body-fixed coordinate frame $\mathcal{B}$. The vehicle is actuated by eight propellers.

rotational degrees-of-freedom are parametrized using a unit quaternion $\boldsymbol{q} = (q_0 \ \boldsymbol{q}_{1:3})$ (see e.g. [17], and references therein). The attitude kinematics are given by

$$\dot{\boldsymbol{q}} = \frac{1}{2}\boldsymbol{q} \cdot \begin{pmatrix} 0 \\ \boldsymbol{\omega} \end{pmatrix}, \tag{12}$$

where $\boldsymbol{\omega}$ denotes the vehicle's body rates and $(\cdot)$ denotes the quaternion multiplication operator.

The vehicle is modeled as a rigid body with mass m and inertia $\boldsymbol{J}$. The translational and rotational dynamics are then given by the Newton-Euler equations:

$$m\ddot{\boldsymbol{p}} = \boldsymbol{R}(\boldsymbol{q})\boldsymbol{f} - m\boldsymbol{g}, \tag{13}$$
$$\boldsymbol{J}\dot{\boldsymbol{\omega}} = \boldsymbol{t} - \boldsymbol{\omega} \times \boldsymbol{J}\boldsymbol{\omega}, \tag{14}$$

where $\boldsymbol{R}(\boldsymbol{q})$ is the rotation matrix that maps a vector from the body-fixed coordinate frame $\mathcal{B}$ to the inertial frame $\mathcal{I}$, $\boldsymbol{g}$ denotes gravity and $\boldsymbol{f}$ and $\boldsymbol{t}$ are defined by (2) and (3), respectively.

IV. CONTROL

In this section, we introduce a control strategy for the vehicle modeled in Section III to simultaneously track a desired position and attitude trajectory $\boldsymbol{p}_{\text{des}}$ and $\boldsymbol{q}_{\text{des}}$, respectively. Because the translational and rotational dynamics are decoupled, the task of tracking position and attitude trajectories is done in two separate control loops. Figure 5 shows the proposed control architecture. First, a desired force and desired body rates are computed by the position and attitude controller, respectively. The desired body rates are subsequently tracked by an inner control loop which outputs desired torques. Finally, the propeller thrusts are chosen such that the desired force and torque are obtained.

A. Position Control

The position tracking controller is chosen such that the dynamics of the position error $\boldsymbol{p}_{\text{err}} = \boldsymbol{p}_{\text{des}} - \boldsymbol{p}$ behave like
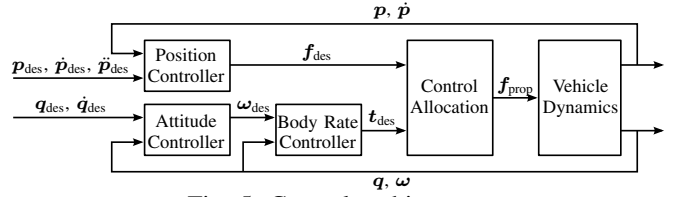

Fig. 5: Control architecture.

a second-order system with time constant τ and damping ratio ζ. An integral term with gain k_{i} is added to reduce the steady-state effects of disturbances and to compensate for modeling errors such as aerodynamic interference between rotors caused by crossing airflows. The desired force is therefore given by:

$$\boldsymbol{f}_{\text{des}} = m\boldsymbol{R}(\boldsymbol{q})^{-1}\bigg(\boldsymbol{g} + \ddot{\boldsymbol{p}}_{\text{des}} + k_{\text{p}}\boldsymbol{p}_{\text{err}}$$
$$+ k_{\text{i}}\int \boldsymbol{p}_{\text{err}}dt + k_{\text{d}}\dot{\boldsymbol{p}}_{\text{err}}\bigg), \tag{15}$$

where the proportional and derivative gains are

$$k_{\text{p}} = \frac{1}{\tau^2} + 2k_{\text{i}}\zeta\tau, \tag{16}$$
$$k_{\text{d}} = \frac{2\zeta}{\tau} + k_{\text{i}}\tau^2. \tag{17}$$

B. Attitude Control

The vehicle's attitude is tracked using a cascaded control structure. First, an outer control loop computes desired body rates $\boldsymbol{\omega}_{\text{des}}$ in order to track the desired attitude. We assume that the desired body rates are perfectly tracked by an inner control loop, such that the rotational dynamics can be neglected when designing the outer loop. In order to be able to exploit the vehicle's omni-directionality, we apply a globally asymptotically stable attitude control law, similar to the one proposed in [18], [19], such that any desired attitude can be tracked. The attitude control law is chosen such that the attitude error dynamics for small errors follow a first-order system with time constant τ_{att}. Let the attitude error be defined as

$$\boldsymbol{q}_{\text{err}} = \boldsymbol{q}^{-1} \cdot \boldsymbol{q}_{\text{des}}. \tag{18}$$

The desired body rates are then

$$\boldsymbol{\omega}_{\text{des}} = \frac{2}{\tau_{\text{att}}}\text{sgn}(q_{\text{err},0})\boldsymbol{q}_{\text{err},1:3} + \boldsymbol{\omega}_{\text{ff}}, \tag{19}$$

where $\boldsymbol{\omega}_{\text{ff}}$ is the body rate feed-forward given by

$$\boldsymbol{\omega}_{\text{ff}} = 2\boldsymbol{q}_{\text{err}} \cdot \boldsymbol{q}_{\text{des}}^{-1} \cdot \dot{\boldsymbol{q}}_{\text{des}} \cdot \boldsymbol{q}_{\text{err}}^{-1}. \tag{20}$$

The sign of the quaternion error in (19) is used to prevent the controller from unnecessarily commanding a rotation of more than 180 degrees.

The inner control loop tracking the desired body rates is designed such that the elements of the angular velocity error behave like a first-order system with time constant τ_{ω}, resulting in a desired torque

$$\boldsymbol{t}_{\text{des}} = \frac{1}{\tau_{\omega}}\boldsymbol{J}(\boldsymbol{\omega}_{\text{des}} - \boldsymbol{\omega}) + \boldsymbol{\omega} \times \boldsymbol{J}\boldsymbol{\omega}. \tag{21}$$

Because the desired body rates are tracked by a high-bandwidth inner control loop, modeling errors in the

rotational dynamics have less effect than in the translational dynamics and therefore no integral control on attitude is applied.

C. Control Allocation

The previously computed desired force and torque need to be converted to propeller thrusts. Because the system is over-actuated there exist multiple propeller thrusts which generate the same force and torque output. One method to obtain a unique relation from forces and torques to propeller thrusts is to use the pseudo-inverse defined by

$$M^\dagger = M^T \left(M M^T \right)^{-1},\tag{22}$$

which minimizes the required control effort to generate the desired force and torque in the least-square sense. The propeller thrusts can then be computed by

$$f_{\text{prop}} = M^\dagger \begin{pmatrix} f_{\text{des}} \\ t_{\text{des}} \end{pmatrix}.\tag{23}$$

Note that allocating the propeller thrusts by using the pseudo-inverse may result in inadmissible propeller thrusts even though the desired force and torque lie in the set of attainable forces and torques. One method to overcome this is to explore the null space of M (see [20], and references therein). However, this is left for further analysis and for the preliminary experimental results presented in Section V the actuator commands are clipped at their saturation limits.

V. RESULTS

In this section, we present the implementation of a proto-type vehicle and experimental results.

A. Implementation

A prototype vehicle with the presented actuator configuration with an edge length of 0.45 m and with the actuator mounted at a distance of 0.184 m from the center of mass is built as shown in Fig. 1. The vehicle consists of a PX4 FMU flight computer [21], communication radios, eight RTF2208 brushless motors with symmetric propellers, eight DYS SN20A electronic speed controllers with SimonK firmware controlling the motors and able to reverse their spinning direction and a four-cell 1800 mAh LiPo battery. The vehicle's frame is constructed using carbon rods due to their stiffness and light weight. 3D printed parts are used to connect the carbon rods in the corners and the center and to carry the electronics and battery. Table I shows a mass breakdown of the vehicle. With a minimum and maximum actuator thrust of $f_{\text{prop,min}} = 0.2$ N and $f_{\text{prop,max}} = 6.7$ N and a total vehicle weight of 0.886 kg, the vehicle is able to accelerate with 24.0 m s^{-2} in any direction if gravity is not considered.

B. Experimental results

The experiments are carried out in the Flying Machine Arena [22], an indoor testbed for aerial vehicles at ETH Zurich. The vehicle's state is estimated using position and attitude data provided by an infrared motion-capture system

TABLE I: Vehicle mass breakdown

Component	Qty	Unit Weight (kg)	Total Weight (kg)
PX4 FMU	1	0.008	0.008
Communication Radio	2	0.008	0.016
Motor	8	0.0455	0.364
Propeller	8	0.0105	0.084
Electronic Speed Controller	8	0.002	0.016
Battery	1	0.196	0.196
Frame	1	0.152	0.152
Wiring	1	0.020	0.020
Others (screws, markers, ...)	1	0.020	0.020
Assembled Vehicle			0.886

and predicted to compensate for the closed-loop latency. The position and outer attitude controller are implemented offboard on a desktop computer, which transmits the desired force and angular rates to the vehicle at a frequency of 50 Hz through a low-latency radio link. The inner body rate controller and the control allocation are implemented onboard and run at a rate of 1000 Hz.

In order to showcase the vehicle's capabilities, two different flight maneuvers are executed. In a first experiment, the vehicle's ability to simultaneously track a position and attitude trajectory is evaluated. The vehicle is commanded to track a horizontal circle of radius 1.5 m at a velocity of 1.95 m s^{-1} while maintaining zero zyx-Euler angles (ψ, θ, ϕ) [17]. The results of this experiment are shown in Fig. 6. The experiment indicates that there exists a coupling between the translational and rotational dynamics which the controller is not able to fully compensate.

The vehicle's omni-directionality is tested in a second experiment by rotating the vehicle about an axis in the horizontal plane while hovering at a fixed position. The tracking errors for this maneuver are shown in Fig. 7. A video showing the experimental results is attached to this submission.

VI. CONCLUSION

An actuator configuration for an omni-directional aerial vehicle has been presented. A simplified force and torque model which does not capture higher-order aerodynamic effects has been used for the design and control of the vehicle. While experiments with a prototype vehicle based on reversible motor-propeller actuators have proven the feasibility of the design approach and the vehicle's capability to independently generate thrust and torque in all directions, they have also indicated that the proposed controller using the simplified force and torque model is not able to fully decouple the vehicle's translational and rotational dynamics.

Future work thus includes the identification of a more detailed thrust and torque map, the development of a control allocation strategy capable of recovering the entire set of attainable forces and torques and the application of learning methods to compensate for the systematic errors shown in the experiments. Furthermore, we intend to investigate the use of the developed platform for physical interaction with the environment and augmented reality.
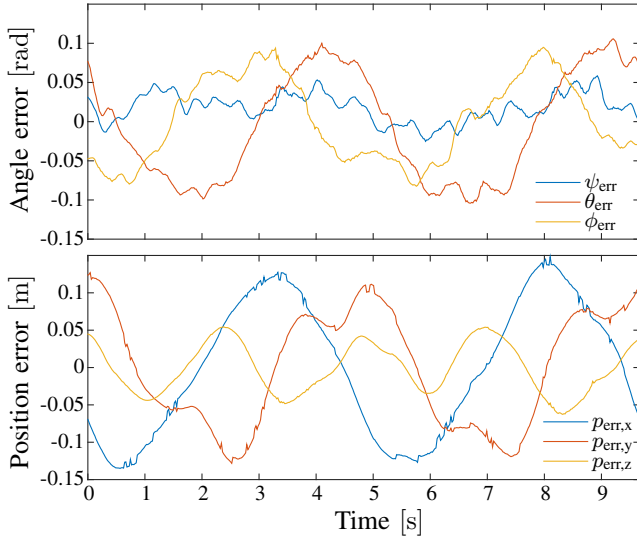
Fig. 6: Position and angle error when tracking a horizontal circle of radius 1.5 m at a velocity of 1.95 m s^{-1} for a duration of two rotations.

Fig. 7: Position and angle error for a rotation about the vehicle's y-axis starting at 2 s. ϑ_err denotes the angular tracking error about the desired rotation axis and φ_err denotes the deflection perpendicular to the rotation axis.

REFERENCES

[1] D. Mellinger, Q. Lindsey, M. Shomin, and V. Kumar, "Design, modeling, estimation and control for aerial grasping and manipulation," in *IEEE/RSJ International Conference on Intelligent Robots and Systems (IROS)*, pp. 2668–2673, Sept 2011.

[2] F. Huber, K. Kondak, K. Krieger, D. Sommer, M. Schwarzbach, M. Laiacker, I. Kossyk, S. Parusel, S. Haddadin, and A. Albu-Schaffer, "First analysis and experiments in aerial manipulation using fully actuated redundant robot arm," in *IEEE/RSJ International Conference on Intelligent Robots and Systems (IROS)*, pp. 3452–3457, Nov 2013.

[3] M. Fumagalli, R. Naldi, A. Macchelli, F. Forte, A. Keemink, S. Stramigioli, R. Carloni, and L. Marconi, "Developing an aerial manipulator prototype: Physical interaction with the environment," *IEEE Robotics Automation Magazine*, vol. 21, pp. 41–50, Sept 2014.

[4] F. Augugliaro, A. Mirjan, F. Gramazio, M. Kohler, and R. D'Andrea, "Building tensile structures with flying machines," in *IEEE/RSJ International Conference on Intelligent Robots and Systems (IROS)*, pp. 3487–3492, Nov 2013.

[5] F. Augugliaro and R. D'Andrea, "Admittance control for physical human-quadrocopter interaction," in *Control Conference (ECC), 2013 European*, pp. 1805–1810, July 2013.

[6] K. Nitta, K. Higuchi, and J. Rekimoto, "Hoverball: Augmented sports with a flying ball," in *Proceedings of the 5th Augmented Human International Conference*, pp. 13:1–13:4, ACM, 2014.

[7] M. Ryll, H. Bulthoff, and P. Giordano, "Modeling and control of a quadrotor uav with tilting propellers," in *IEEE International Conference on Robotics and Automation (ICRA)*, pp. 4606–4613, May 2012.

[8] C. Papachristos, K. Alexis, and A. Tzes, "Efficient force exertion for aerial robotic manipulation: Exploiting the thrust-vectoring authority of a tri-tiltrotor uav," in *IEEE International Conference on Robotics and Automation (ICRA)*, pp. 4500–4505, May 2014.
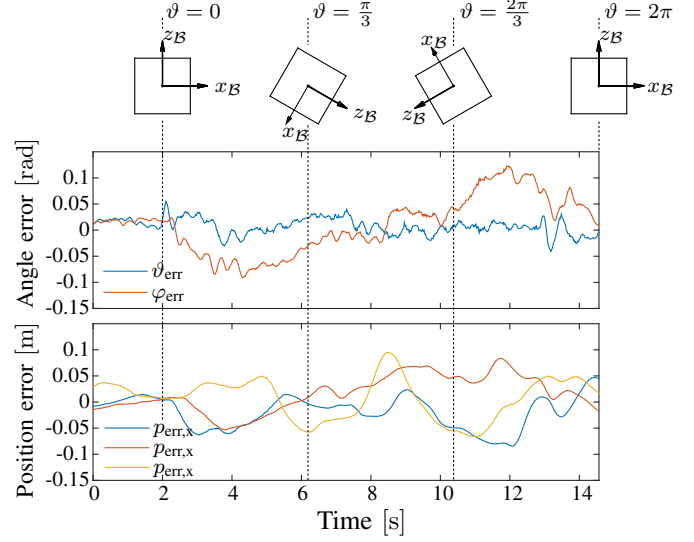
[9] Y. Long and D. Cappelleri, "Omnicopter: A novel overactuated micro aerial vehicle," in *Advances in Mechanisms, Robotics and Design Education and Research*, vol. 14 of *Mechanisms and Machine Science*, pp. 215–226, Springer International Publishing, 2013.

[10] B. Crowther, A. Lanzon, M. Maya-Gonzalez, and D. Langkamp, "Kinematic analysis and control design for a nonplanar multirotor vehicle," *Journal of Guidance, Control, and Dynamics*, vol. 34, no. 4, pp. 1157–1171, 2011.

[11] G. Jiang and R. Voyles, "Hexrotor uav platform enabling dextrous interaction with structures-flight test," in *IEEE International Symposium on Safety, Security, and Rescue Robotics (SSRR)*, pp. 1–6, Oct 2013.

[12] E. Kaufman, K. Caldwell, D. Lee, and T. Lee, "Design and development of a free-floating hexrotor uav for 6-dof maneuvers," in *IEEE Aerospace Conference*, pp. 1–10, March 2014.

[13] S. Rajappa, M. Ryll, H. H. Bülthoff, and A. Franchi, "Modeling, control and design optimization for a fully-actuated hexarotor aerial vehicle with tilted propellers," in *IEEE International Conference on Robotics and Automation (ICRA)*, May 2015.

[14] A. Nikou, G. C. Gavridis, and K. J. Kyriakopoulos, "Mechanical design, modelling and control of a novel aerial manipulator," in *IEEE International Conference on Robotics and Automation (ICRA)*, pp. 4698–4703, May 2015.

[15] P. K. Aravind, "A comment on the moment of inertia of symmetrical solids," *American Journal of Physics*, vol. 60, pp. 754–755, Aug. 1992.

[16] F. Cotton, *Chemical applications of group theory*. A Wiley interscience publication, Wiley, 1990.

[17] J. Diebel, "Representing attitude: Euler angles, unit quaternions, and rotation vectors," *Matrix*, vol. 58, pp. 15–16, 2006.

[18] D. Brescianini, M. Hehn, and R. D'Andrea, "Nonlinear quadrocopter attitude control," tech. rep., ETH Zurich, 2013.

[19] C. Mayhew, R. Sanfelice, and A. Teel, "Quaternion-based hybrid control for robust global attitude tracking," *IEEE Transactions on Automatic Control*, vol. 56, pp. 2555–2566, Nov 2011.

[20] M. Bodson, "Evaluation of optimization methods for control allocation," *Journal of Guidance, Control, and Dynamics*, vol. 25, pp. 703–711, July 2002.

[21] L. Meier, D. Honegger, and M. Pollefeys, "PX4: A node-based multithreaded open source robotics framework for deeply embedded platforms," in *IEEE International Conference on Robotics and Automation (ICRA)*, May 2015.

[22] S. Lupashin, M. Hehn, M. W. Mueller, A. P. Schoellig, M. Sherback, and R. DAndrea, "A platform for aerial robotics research and demonstration: The flying machine arena," *Mechatronics*, vol. 24, no. 1, pp. 41 – 54, 2014.